Supporting Information

Role of *d* Elements in a Proton–Electron Coupling of *d*–π Hybridized Electron Systems

Mikihiro Hayashi,*†‡ Yuki Takahashi, † Yukihiro Yoshida,† Kunihisa Sugimoto,‖ and Hiroshi Kitagawa*†

†*Division of Chemistry, Graduate School of Science, Kyoto University, Kitashirakawa-Oiwakecho, Sakyo-ku, Kyoto 606-8502, Japan*

‡*Faculty of Education, Nagasaki University, 1-14 Bunkyo-machi, Nagasaki 852-8521, Japan*

‖*Japan Synchrotron Radiation Research Institute (JASRI), SPring-8, 1-1-1 Kouto, Sayo-cho, Sayo-gun, Hyogo 679-5198, Japan*

Contents

S.1. Experimental details

S.1.1 Materials

Pyrazine-2,3-dithiol (**H_2L**) was prepared according to the previous report.[1] In the synthesis, nickel(II) chloride hexahydrate ($NiCl_2{\cdot}6H_2O$), potassium tetrachloropalladate(II) (K_2PdCl_4), potassium tetrachloroplatinate(II) (K_2PtCl_4), sodium hydroxide (NaOH), hydrochloric acid (HCl), trifluoroacetic acid (TFA), tetrabutylammonium bromide (TBABr), acetone, diethyl ether, iodine (I_2), dichloromethane (CH_2Cl_2), ethanol, and ethylenediammonium dichloride ($(CH_2NH_3)_2Cl_2$) (FUJIFILM Wako Pure Chemical Corp.) were used without any purification. Water was purified by ion exchange columns. *N*,*N*-Dimethylformamide (DMF), pyridine (Py), (FUJIFILM Wako Pure Chemical Corp.) were used of the commercially available grade. In Infrared (IR) spectroscopic measurements, KBr (crystal block) (FUJIFILM Wako Pure Chemical Corp.) was utilized as diluting agents. In pH-dependent measurements, sodium perchlorate monohydrate ($NaClO_4{\cdot}H_2O$) (Nacalai Tesque, Inc.) and 0.05 mM acetic acid–sodium acetate solution (FUJIFILM Wako Pure Chemical Corp.) were utilized for buffer solutions, whereas sodium hydroxide and perchloric acid (60%) (FUJIFILM Wako Pure Chemical Corp.) were adopted to modify the pH condition. In electrochemical measurements, DMF, dimethylsulfoxide (DMSO) (FUJIFILM Wako Pure Chemical Corp., infinity pure grade), ferrocene (FUJIFILM Wako Pure Chemical Corp.), and tetrabutylammonium perchlorate ($TBAClO_4$) (Nacalai Tesque, Inc., special prepared reagent) were used. In the acid addition experiments, bis(trifluoromethanesulfonyl)amine (HTFSA) (Sigma-Aldrich Co. LLC.) was used as a proton source. In ^{1}H NMR measurements, DMSO-d_6 (Tokyo Chemical Industry Co., Ltd.) was adopted.

S.1.2 Experiments

S.1.2.1 X-ray diffraction measurements of single crystals

The diffraction data of single crystals of **Ni(HL)$_2$**, **Pd(HL)$_2$**, and **Pt(HL)$_2$** were collected by use of the synchrotron X-ray (λ = 0.5592 Å) at the BL02B1 beamline in SPring-8 with the imaging plate system. In addition, the diffraction data of single crystals of Ni and Pt complexes, **Ni(HL)$_2$**, **TBA$_2$[Ni(L)$_2$]**, **TBA[Ni(L)$_2$]**, **TBA[Ni(HL)(L)]**, and **TBA[Pt(HL)(L)]**, were collected at 100 K by using a Bruker SMART APEX II CCD area detector with a graphite–monochromated Mo *K*α radiation. Empirical absorption corrections using equivalent reflections and Lorentzian polarization correction were performed using the program Crystal Clear 3.8.0 or the free GUI software Yadokari-XG 2009. The structures were refined on F^2 using SHELXL-97 or SHELEX-2018/1.

S.1.2.2 Spectroscopic measurements

The data of IR absorbances of Ni complexes, **Ni(HL)$_2$**, **TBA$_2$[Ni(L)$_2$]**, **TBA[Ni(L)$_2$]**, and **TBA[Ni(HL)(L)]**, were collected by a ThermoNicolet NEXUS 670 FT-IR spectrometer. KBr was used for a diluting agent for all samples. Electronic absorption spectra of all complexes were measured by a Jasco V-570 UV/Vis spectrometer. Except for pH-dependent measurements, DMSO was used for a solvent.

S.1.2.3 Theoretical calculations

The three-parameterized Becke-Lee-Yang-Parr (B3LYP) hybrid exchange-correlation function was employed. As a basis set, 6-31+G(d,p) (C, H, N, and S) and Lanl2dz (Ni, Pd, and Pt) were used for all complexes. The *trans*-type geometry of di-protonated structure was selected for a comparison of HOMO energy level among **M(HL)$_2$** (M = Ni, Pd, and Pt). Time-dependent DFT (TD-DFT) calculations were executed under the same condition. These optimized structures were utilized in the NBO analyses. Solvent effects were not considered in any processes. These calculations were implemented with the Gaussian 03 program.

S.1.2.4 Electron spin resonance measurements

X-band electron spin resonance (ESR) spectra of polycrystalline **TBA[Ni(L)$_2$]** were recorded at 287 K with a Bruker EMX EPR spectrometer.

S.1.2.5 Preparation conditions of pH

Adding an aqueous solution of $NaClO_4$ to the aqueous solution of AcOH–NaOAc provided an aqueous buffer solution satisfied with following concentrations: 0.1 M $NaClO_4$ and 0.01 M

NaOAc. The pH-dependent absorption measurements of **M(HL)$_2$** (M = Ni, Pd, and Pt) were performed in a DMSO/aqueous (1:1, v/v) buffer solution. In case of electrochemical measurements, a DMSO/aqueous (3:1, v/v) buffer solution was used. In both measurements, the concentration of metal complexes was 0.1 mM. Values of pH modified by adding aqueous solutions of NaOH or $HClO_4$ were monitored by the Custom PH-5011A pH meter.

S.1.2.6 Electrochemical measurements

A series of electrochemical measurements was carried out in a standard one-component cell, using a 3mmΦ glassy carbon (BAS Inc.) as a working electrode, a platinum wire (BAS Inc.) as a counter electrode, and an in-house made Ag/$AgClO_4$ reference electrode (0.01 M $AgClO_4$ in 0.1 M $TBAClO_4$/acetonitrile). As an internal standard, a redox couple of ferrocene was utilized in each measurement. Electrochemical data were acquired with an ALS CHI720 and 650B electrochemical analyzers (BAS Inc.). Except for pH-dependent measurements, DMSO was used for a solvent.

S.1.2.7 NMR measurement

NMR spectroscopic measurements of Ni complexes in DMSO-d_6 were performed by a JEOL spectrometer at 600MHz.

S.2. Synthetic details

S.2.1 Synthesis of **M(HL)$_2$** (M = Ni, Pd, and Pt)

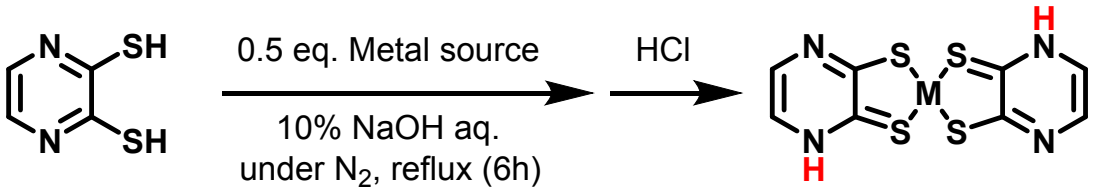

Scheme S1. Complex formation and protonation reactions.

Ni(HL)$_2$: Under N_2 atmosphere, $NiCl_2 \cdot 6H_2O$ (0.43 g, 1.78 mmol) was added to a solution of **H_2L** (0.5 g, 3.47 mmol) in NaOH aq. (500 mL). After refluxing the mixture for 6 hours, a precipitate was filtered off. Addition of small amount of HCl into the filtrate provided the protonated Ni complex as purple powder. The powder was recrystallized from the DMF solution with a small amount of TFA, which afforded single crystals of **Ni(HL)$_2$**. The obtained single crystals of **Ni(HL)$_2$** contained the equal amount of DMF molecules as crystal solvents. (77% as a synthetic yield).

Elem. Anal. Found (Calcd) for $C_{11}H_{13}N_5NiOS_4$ (%): C 31.48 (31.59), H 3.08 (3.13), N 16.72 (16.76).

Pd(HL)$_2$ and **Pt(HL)$_2$**: Under N_2 atmosphere, a metal source (K_2PdCl_4: 0.57 g, 1.78 mmol; K_2PtCl_4: 0.73 g, 1.78 mmol) was added to a solution of **H_2L** (0.5 g, 3.47 mmol) in NaOH aq. (500 mL). After refluxing the mixture for 6 hours, a precipitate was filtered off. Addition of small amount of HCl into the filtrate provided the protonated Pd or Pt complexes as red or blue-purple powder. The powder was recrystallized from the Py solution with a small amount of TFA, which afforded single crystals of **Pd(HL)$_2$** (85% as a synthetic yield) or **Pt(HL)$_2$** (98% as a synthetic yield). These single crystals contained twice amounts of Py molecules as crystal solvents.

Elem. Anal. Found (Calcd) for $C_{18}H_{16}N_6PdS_4$ (%): C 39.77 (39.23), H 2.94 (2.93), N 14.73 (15.25). Found (Calcd) for $C_{18}H_{16}N_6PtS_4$ (%): C 32.30 (33.80), H 2.33 (2.52), N 12.71 (13.14).

S.2.2 Synthesis of **(TBA)$_2$[M(L)$_2$]** (M = Ni and Pt)

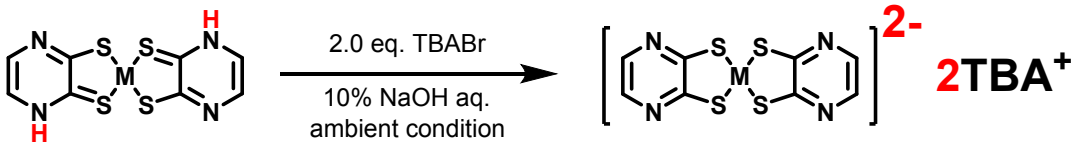

Scheme S2. Cation exchange reaction.

Under the ambient condition, **M(HL)$_2$** (M = Ni and Pt) (1.0 mmol) was dissolved in an aqueous solution of NaOH (300 mL) and two equivalent amounts of TBABr (0.65 g) was added to the solution. Stirring the solution provided a deprotonated complex as a precipitate. Polycrystalline powder of **(TBA)$_2$[M(L)$_2$]** was obtained by exposing their acetone solutions to diethyl ether vapor (60% in the Ni complex and 94% in the Pt complex as a synthetic yield). Elem. Anal. Found (Calcd) for $C_{40}H_{72}N_6NiS_4$ (%): C 57.79 (58.02), H 9.27 (9.25), N 10.15 (10.15). Found (Calcd) for $C_{40}H_{72}N_6PtS_4$ (%): C 49.34 (49.82), H 7.82 (7.94), N 8.74 (8.71).

S.2.3 Synthesis of **TBA[M(HL)(L)]** (M = Ni and Pt)

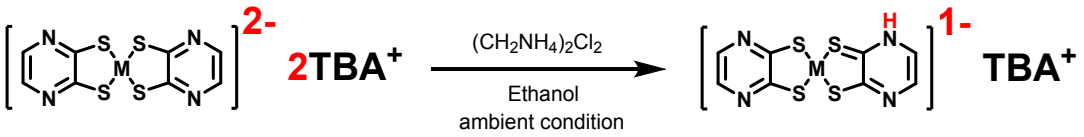

Scheme S3. Singly protonation reaction of Ni complex.

Under the ambient condition, **(TBA)$_2$[Ni(L)$_2$]** (1.0 g, 1.2 mmol) dissolved in ethanol (300 mL) was slowly exposed to a saturated aqueous solution of $(CH_2NH_3)_2Cl_2$ by using a liquid-liquid interface. After one week, block-shaped single crystals of the monoprotonated complex (**TBA[Ni(HL)(L)]**) were grown in the solution. In case of the Pt complex, a small amount of single crystals of **TBA[Pt(HL)(L)]** was obtained by the slow diffusion of $(CH_2NH_3)_2Cl_2$ aq. into an ethanol solution of **TBA[Pt(HL)(L)]**.

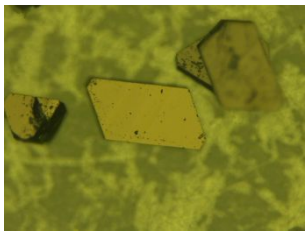

Figure S1. Picture of crystals of **TBA[Ni(HL)(L)]**.

Elem. Anal. Found (Calcd) for $C_{24}H_{41}N_5NiS_4$ (%): C 49.10 (49.14), H 7.11 (7.05), N 11.92 (11.93).

S.2.4 Synthesis of **TBA[Ni(L)$_2$]**

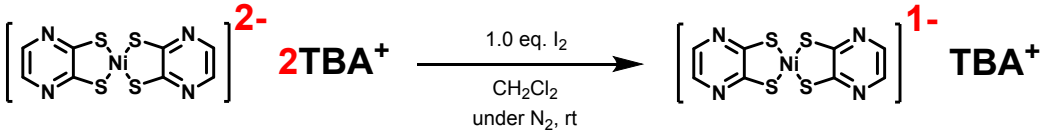

Scheme S4. Iodine-oxidation of Ni complex.

Under N_2 atmosphere, **(TBA)$_2$[Ni(L)$_2$]** (500 mg, 0.604 mmol) was dissolved in CH_2Cl_2 (20 mL) and an equivalent amount of

Figure S2. Picture of crystals of **TBA[Ni(L)$_2$]**.

I_2 (154 mg, 0.607 mmol) was added to the solution. Stirring the solution changed the color from brown to green, and a precipitate was filtered off. After evaporation of CH_2Cl_2 under reduced pressure, a black powder of the mono-oxidized Ni complex was obtained. Needle-shaped single crystals were grown by exposing its acetone solution to diethyl ether vapor (85% as a synthetic yield).

Elem. Anal. Found (Calcd) for $C_{24}H_{40}N_5NiS_4$ (%): C 49.18 (49.23), H 6.81 (6.89), N 11.89 (11.96).

S.3 Crystal structures

S.3.1 Crystal structures of **TBA[Ni(HL)(L)]**, **TBA[Ni(L)$_2$]**, **Pd[HL]$_2$·2Py**, and **TBA[Pt(HL)(L)]**.

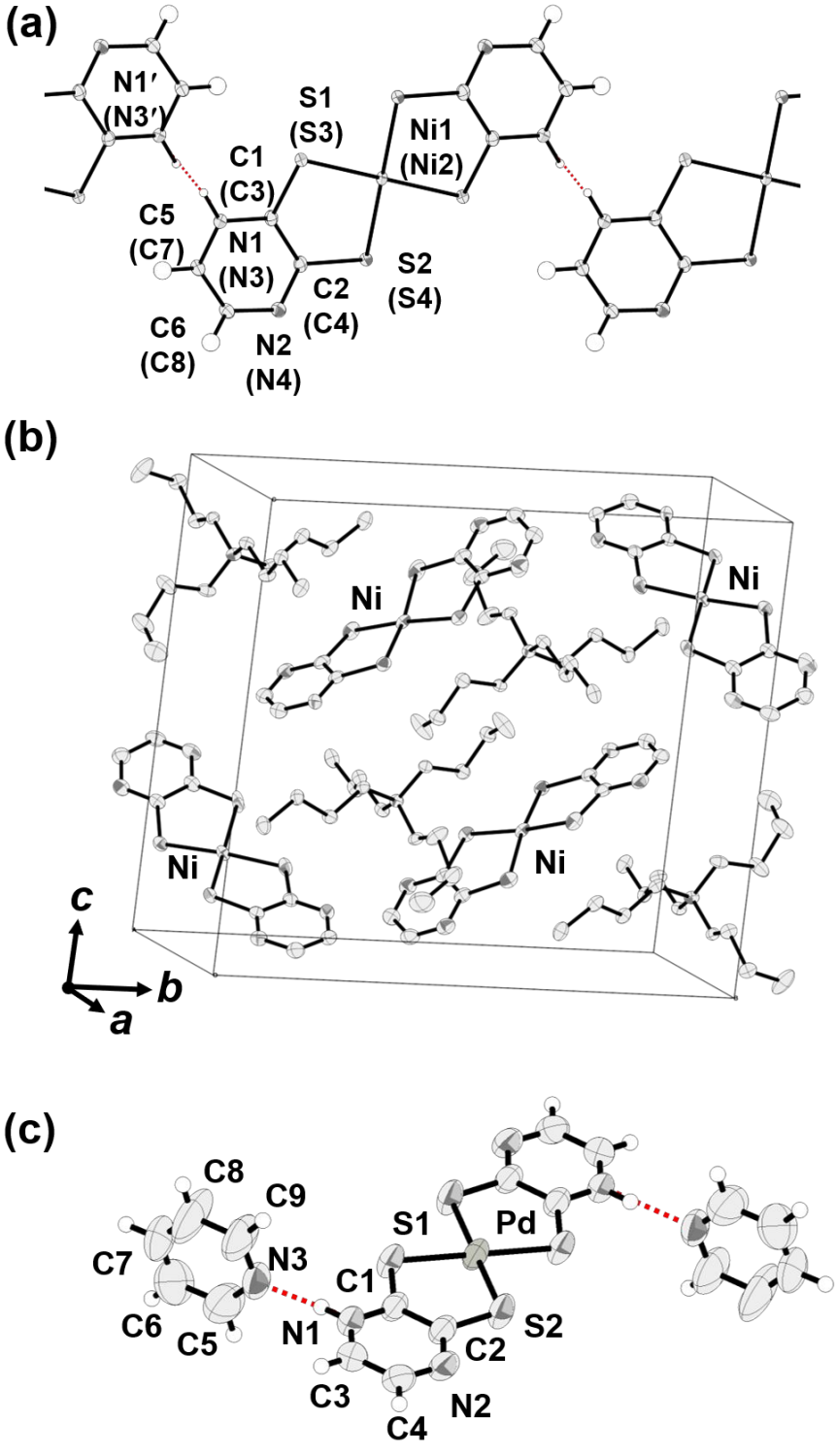

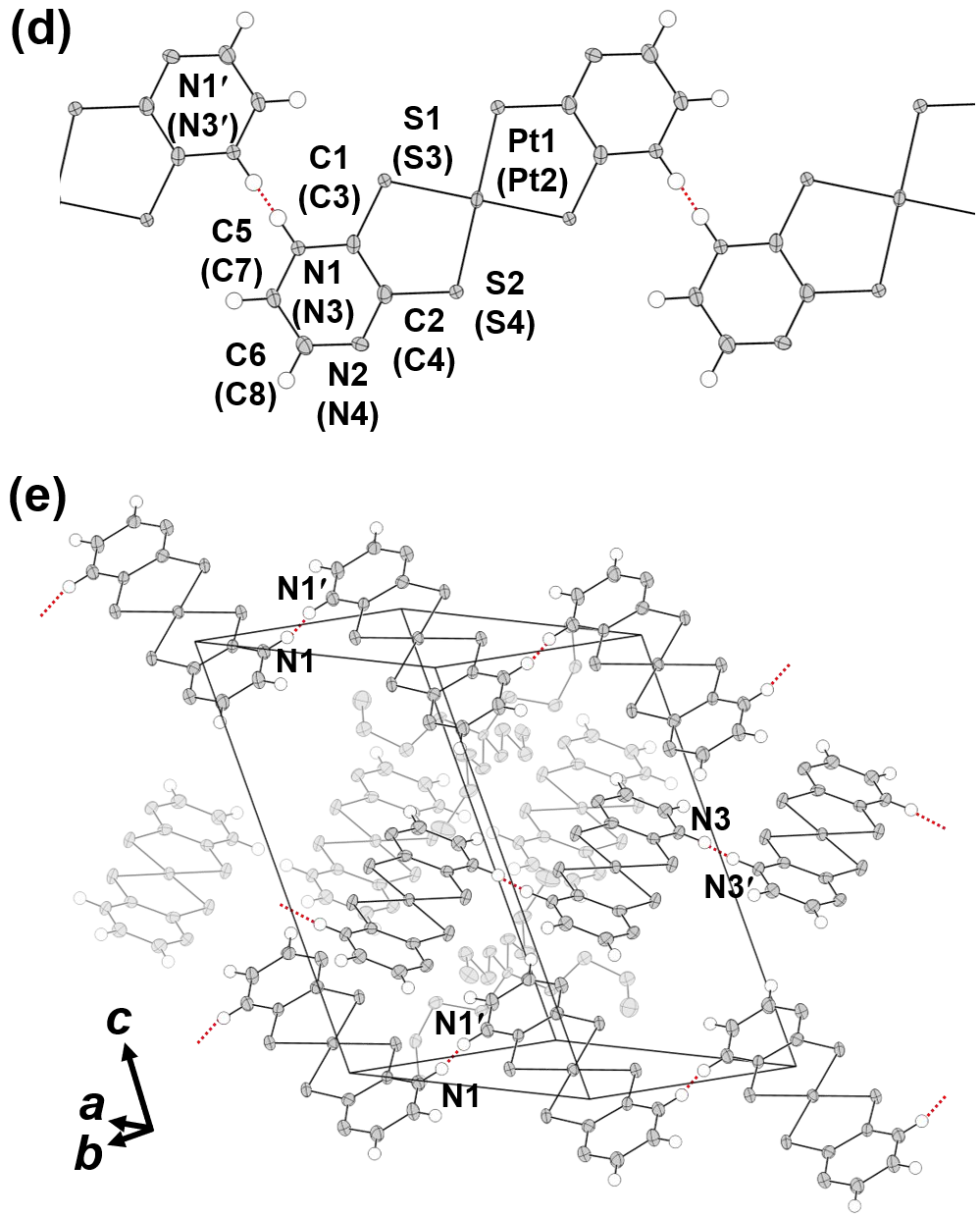

Figure S3. ORTEP drawings of **TBA[Ni(HL)(L)]** (a), **TBA[Ni(L)$_2$]** (b), **Pd(HL)$_2$·2Py** (c), and **TBA[Pt(HL)(L)]** (d), (e) with thermal ellipsoids drawn at 50% probability. Hydrogen atoms containing TBA ions were omitted for clarity. In (a), (c), (d), and (e), H-bonds of the N–H···N types are shown as dotted lines. In crystal structures of **TBA[Ni(HL)(L)]** and **TBA[Pt(HL)(L)]**, the protonated positions of nitrogen atoms are disordered.

S.3.2 Crystallographic data

Table S1. Crystallographic data of the diprotonated state of complexes obtained in this study

	Ni(HL)$_2$·DMF	**Ni(HL)$_2$·DMF**	**Pd(HL)$_2$·2Py**	**Pt(HL)$_2$·2Py**
Empirical formula	$C_{11}H_{13}N_5ONiS_4$	$C_{11}H_{13}N_5ONiS_4$	$C_{18}H_{16}N_6PdS_4$	$C_{18}H_{16}N_6PtS_4$
Formula weight	418.21	418.21	551.05	639.69
Color and habit	brown, block	brown, block	red, prism	red, block
T / K	296	100	296	296
Wavelength / Å	0.5592	0.71075	0.5592	0.5592
Crystal system	Monoclinic	Monoclinic	Monoclinic	Monoclinic
space group	$P2_1$	Cc	$P2_1/a$	$P2_1/a$
a / Å	6.6990(10)	6.576(2)	9.1160(7)	9.2910(10)
b / Å	9.9020(13)	24.360(8)	11.6900(9)	11.5040(15)
c / Å	12.655(8)	9.895(3)	10.8200(5)	10.8800(10)
α / deg	-	-	-	-
β / deg	105.339(10)	90.107(4)	104.803(4)	104.696(7)
γ / deg	-	-	-	-
V / Å^3	809.5(5)	1585.0(9)	1114.78(13)	1124.9(2)
Z	2	4	2	2
Crystal size / mm	0.20 x 0.05 x 0.05	0.10 x 0.05 x 0.05	0.20 x 0.10 x 0.10	0.20 x 0.05 x 0.05
$D_{calc.}$ / g cm^{-3}	1.715	1.753	1.641	1.889
μ / cm^{-1}	1.720	1.757	1.225	6.600
F(000)	428	856	552	616
Independent reflections	4039	3694	3342	3291
R_1, wR_2 [$I > 2\sigma(I)$]	0.0633, 0.1311	0.0466, 0.0847	0.0472, 0.1398	0.0625, 0.1904
GOF	1.086	1.000	1.131	1.149

Table S2. Crystallographic data of Ni and Pt complexes obtained in this study

	$(TBA)_2[Ni(L)_2]$	**TBA[Ni(HL)(L)]**	**$TBA[Ni(L)_2]$**	**TBA[Pt(HL)(L)]**
Empirical formula	$C_{40}H_{76}N_6NiS_4$	$C_{24}H_{41}N_5NiS_4$	$C_{24}H_{40}N_5NiS_4$	$C_{24}H_{41}N_5PtS_4$
Formula weight	828.01	586.56	585.55	586.56
Color and habit	red, block	brown, block	green, needle	brown, block
T / K	100	100	100	100
Wavelength / Å	0.71075	0.71069	0.71073	0.71069
Crystal system	Monoclinic	Triclinic	Monoclinic	Triclinic
space group	$P2_1/n$	P-1	$P2_1/c$	P-1
a / Å	7.7723(7)	9.8084(13)	9.2903(12)	9.9538(13)
b / Å	20.4416(18)	10.0948(13)	18.511(2)	10.2166(13)
c / Å	14.1183(12)	15.219(2)	16.684(2)	15.106(2)
α / deg	-	72.7210(10)	-	72.1810(10)
β / deg	96.383(3)	79.4010(10)	95.773(2)	80.2240(10)
γ / deg	-	89.3780(10)	-	89.5660(10)
V / Å^3	2229.2(3)	1412.8(3)	2854.6(6)	1439.6(3)
Z	2	2	4	2
Crystal size / mm	0.50 x 0.10 x 0.10	0.50 x 0.50 x 0.10	0.10 x 0.10 x 0.50	0.10 x 0.10 x 0.50
$D_{calc.}$ / g cm^{-3}	1.234	1.379	1.362	1.668
μ / cm^{-1}	0.657	1.005	0.994	5.186
F(000)	900	624	1244	724
Independent reflections	4071	6519	6450	6519
R_1, wR_2 [$I > 2\sigma(I)$]	0.0319, 0.0831	0.0402, 0.0975	0.0411, 0.1000	0.0370, 0.0976
GOF	1.030	1.391	1.012	1.371

S.3.3 Structural information of metal complexes

Table S3. Values of bond lengths (in Å) and bond angles (in deg) of the diprotonated species, **Ni(HL)$_2$**, **Pd(HL)$_2$**, and **Pt(HL)$_2$**, evaluated from the crystallographic data

	Ni(HL)$_2$ @ 296 K	**Ni(HL)$_2$ @ 100 K**	**Pd(HL)$_2$**	**Pt(HL)$_2$**
M-S(1)	2.159(2)	2.163(3)	2.2877(7)	2.287(2)
M-S(2)	2.1589(19)	2.171(2)	2.2869(9)	2.271(3)
M-S(3)	2.1741(17)	2.171(2)		
M-S(4)	2.163(2)	2.173(3)		
S(1)-C(1)	1.684(6)	1.695(8)	1.714(3)	1.708(11)
S(2)-C(2)	1.752(7)	1.722(7)	1.731(3)	1.759(9)
S(3)-C(3)	1.686(5)	1.706(7)		
S(4)-C(4)	1.732(7)	1.724(8)		
C(1)-C(2)	1.425(9)	1.445(10)	1.423(3)	1.403(11)
C(3)-C(4)	1.428(8)	1.444(10)	1.363(4)	1.385(15)
C(1)-N(1)	1.342(8)	1.347(9)	1.341(4)	1.342(12)
C(2)-N(2)	1.305(9)	1.328(9)	1.331(4)	1.343(14)
C(3)-N(3)	1.339(8)	1.341(10)		
C(4)-N(4)	1.334(9)	1.327(9)		
C(5)-C(6)	1.369(10)	1.380(10)		
C(7)-C(8)	1.399(11)	1.347(11)		
N(1)-H•••O(1)	2.750(7)	2.749(7)		
N(1)-H•••N(3)			2.686(3)	2.717(11)
N(2)-H•••N(3)	2.842(7)	2.829(8)		
∠C(1)-N(1)-C(3)			121.1(3)	119.7(8)
∠C(2)-N(2)-C(4)			118.6(2)	117.6(8)
∠C(1)-N(1)-C(5)	123.3(6)	123.0(7)		
∠C(2)-N(2)-C(6)	118.0(6)	118.7(7)		
∠C(3)-N(3)-C(7)	122.7(6)	121.7(6)		
∠C(4)-N(4)-C(8)	118.4(7)	117.6(7)		

Table S4. Values of bond lengths (in Å) and bond angles (in deg) of Ni and Pt complexes: **$[Ni(L)_2]^{2-}$**, **$[Ni(HL)(L)]^{1-}$**, **$[Ni(L)_2]^{1-}$**, and **$[Pt(HL)(L)]^{1-}$** evaluated from the crystallographic data

	$[Ni(L)_2]^{2-}$	**$[Ni(HL)(L)]^{1-}$**		**$[Ni(L)_2]^{1-}$**	**$[Pt(HL)(L)]^{1-}$**	
M-S(1)	2.1755(4)	2.1628(7)		2.1466(7)	2.2898(13)	
M-S(2)	2.1756(4)	2.1813(7)		2.1592(6)	2.3011(14)	
M-S(3)			2.1786(7)	2.1540(8)		2.2848(15)
M-S(4)			2.1829(7)	2.1548(7)		2.3039(15)
S(1)-C(1)	1.7448(19)	1.712(3)		1.735(3)	1.719(6)	
S(2)-C(2)	1.7370(18)	1.738(3)		1.738(3)	1.740(6)	
S(3)-C(3)			1.723(3)	1.729(3)		1.714(6)
S(4)-C(4)			1.733(3)	1.743(3)		1.729(7)
C(1)-C(2)	1.429(3)	1.428(4)		1.405(4)	1.436(8)	
C(3)-C(4)	1.371(3)		1.439(4)	1.407(4)		1.439(8)
C(1)-N(1)	1.332(2)	1.351(4)		1.338(4)	1.342(7)	
C(2)-N(2)	1.338(3)	1.332(4)		1.340(4)	1.341(7)	
C(3)-N(3)			1.338(3)	1.346(4)		1.347(8)
C(4)-N(4)			1.329(3)	1.339(4)		1.333(8)
C(5)-C(6)		1.366(4)		1.386(5)	1.371(9)	
C(7)-C(8)			1.367(4)	1.380(5)		1.364(9)
N(1)-H•••O(1)						
N(1)-H•••N(1)′		2.760(2)			2.795(8)	
N(2)-H•••N(3)′						
N(3)-H•••N(3)′			2.777(4)			2.795(7)
∠C(1)-N(1)-C(3)	116.07(17)					
∠C(2)-N(2)-C(4)	115.82(17)					
∠C(1)-N(1)-C(5)		119.6(2)		115.8(2)	120.3(5)	
∠C(2)-N(2)-C(6)		117.3(2)		115.7(2)	117.5(5)	
∠C(3)-N(3)-C(7)			119.4(2)	115.6(2)		119.7(5)
∠C(4)-N(4)-C(8)			117.0(2)	115.5(2)		118.1(5)

Table S5. Values of bond angles and bond lengths of the diprotonated species, **$Ni(HL)_2$**, **$Pd(HL)_2$**, and **$Pt(HL)_2$**, estimated from the crystallographic data measured at 296 K

	$Ni(HL)_2$	**$Pd(HL)_2$**	**$Pt(HL)_2$**
$\angle_{C-N-C}$ / °	122.3(6) 118.2(4)	121.1(3) 118.6(2)	119.7(8) 117.6(3)
d_{C-S} / Å	1.685(5) 1.742(20)	1.714(3) 1.731(4)	1.708(11) 1.759(9)

S.4 Spectroscopic measurements

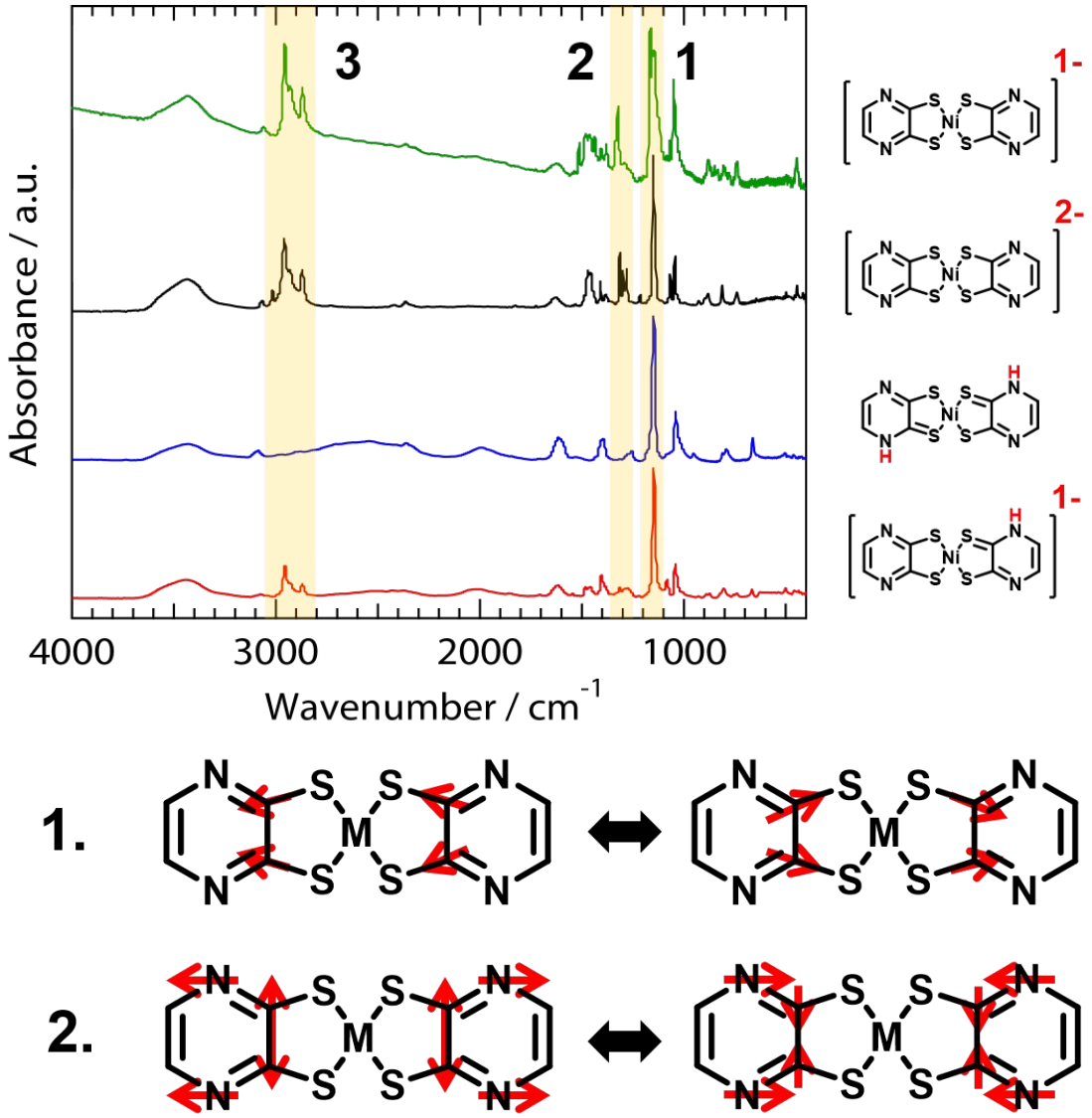

Figure S4. IR spectra of Ni complexes: **Ni(HL)$_2$** (blue), **(TBA)$_2$[Ni(L)$_2$]** (black), **TBA[Ni(L)$_2$]** (green), and **TBA[Ni(HL)(L)]** (red). Three characteristic bands were highlighted in yellow. Bands **1** and **2** correspond to asymmetric and symmetric stretching vibrations indicated by schematic images. Band **3** is assigned to the aliphatic C–H stretching vibration of TBA ion.

S.5 Magnetic measurements

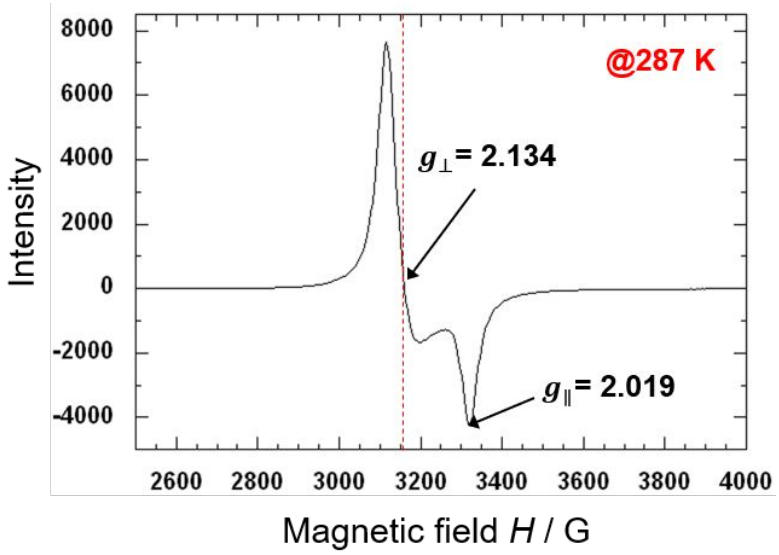

Figure S5. ESR spectrum of polycrystalline **(TBA)[Ni(L)$_2$]** measured at 287 K. Arrows indicate two anisotropic g-values.

S.6 Theoretical calculations

S.6.1 HOMO of **[M(HL)(L)]$^{1-}$** and **[M(L)$_2$]$^{2-}$** (M = Pd and Pt)

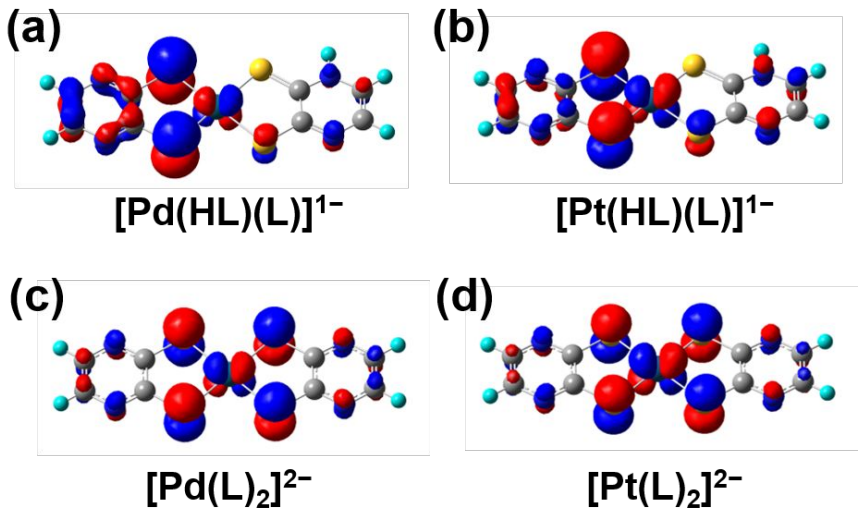

Figure S6. Calculated images of HOMO (Ψ_{82}) of Pd and Pt complexes.

S.6.2 Results of TD-DFT calculations of Ni, Pd, and Pt complexes

Table S6. Averaged values of compositions of *d*- and π-orbitals in antibonding NBO in M–S bonds of Ni, Pd, and Pt complexes. A schematic image of the interaction between lone pair of S atom (blue) and antibonding *d*–π hybridized orbital (red) is shown at the bottom of the table

	M(HL)$_2$ d/π	**[M(HL)(L)]$^{1-}$** d/π	**[M(L)$_2$]$^{2-}$** d/π
Ni	80/20	76/24	80/20
Pd	77/23	73/27	77/23
Pt	73/27	71/29	73/27

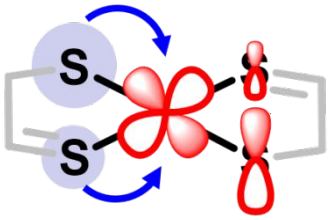

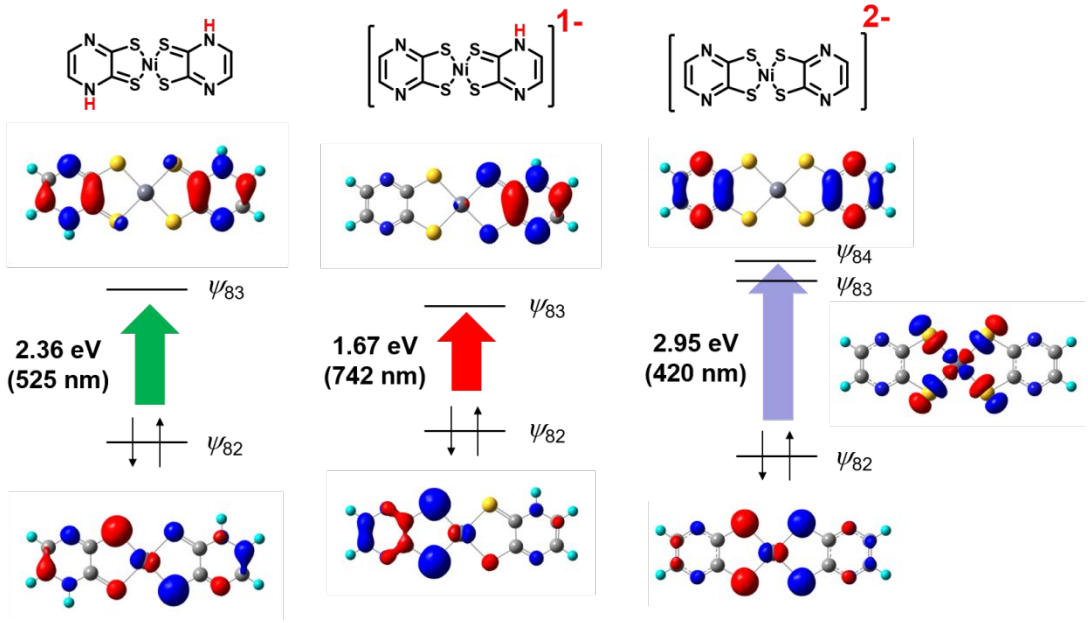

Figure S7. Images of molecular orbitals of non-oxidized Ni complexes. Ψ_{82}, Ψ_{83}, and Ψ_{84} corresponds to HOMO, LUMO, and LUMO+1, respectively. Thick arrows indicate the electronic transitions assigned by the TD-DFT calculations.

Table S7. Calculated energies (in eV) corresponding to the mixed metal-ligand to ligand charge transfer (MMLLCT) in Ni, Pd, and Pt complexes

	$M(HL)_2$ $\Psi_{82} \rightarrow \Psi_{83}$	**$[M(HL)(L)]^{1-}$** $\Psi_{82} \rightarrow \Psi_{83}$	**$[M(L)_2]^{2-}$** $\Psi_{82} \rightarrow \Psi_{84}$
Ni	2.30	1.67	2.95
Pd	2.30	1.60	2.90
Pt	2.03	1.51	2.63*

*MMLLCT of **$[Pt(L)_2]^{2-}$** is assigned to a transition from Ψ_{82} to Ψ_{83} orbitals.

S.7 pH-dependent measurements

S.7.1 pH-dependent electronic absorption of the Pd complex

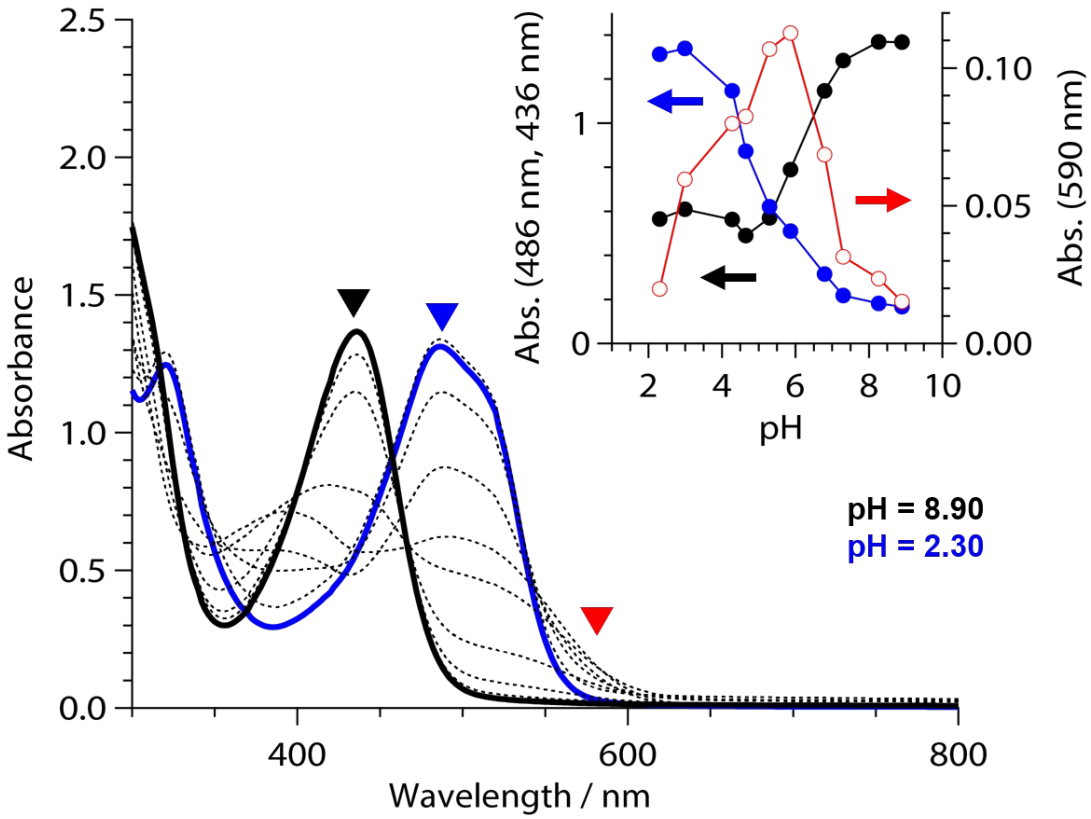

Figure S8. Electronic absorption spectra of the Pd complex under several pH conditions. Blue and black lines are spectra measured at the most acidic and basic conditions, respectively. In the acidic region of pH (2.30 – 5.29), an intense band ($\lambda_{max} =$ 486 nm) indicated by a blue triangle becomes weak and a new absorption band appears in lower energy region assigned by a red triangle with two isosbestic points at 420 and 550 nm. In the slightly basic region of pH (5.86 – 8.90), only an absorbance at 436 nm indicated by a black triangle becomes intense with a new isosbestic point at 470 nm. Successive change in the position of isosbestic point and an appearance of adsorption band corresponding to the mono-protonated state within an intermediate pH range indicates a stepwise protonation of the Pd complex. Inset shows pH-dependence of absorbance monitored at energies corresponding to three triangles. Black and blue filled circles represent traces of absorbance associated with **$[Pd(L)_2]^{2-}$** and **$Pd(HL)_2$**, whereas red open circles represent a trace of absorbance of **$[Pd(HL)(L)]^{1-}$**.

S.7.2 pH-potential diagram of Pd complexes

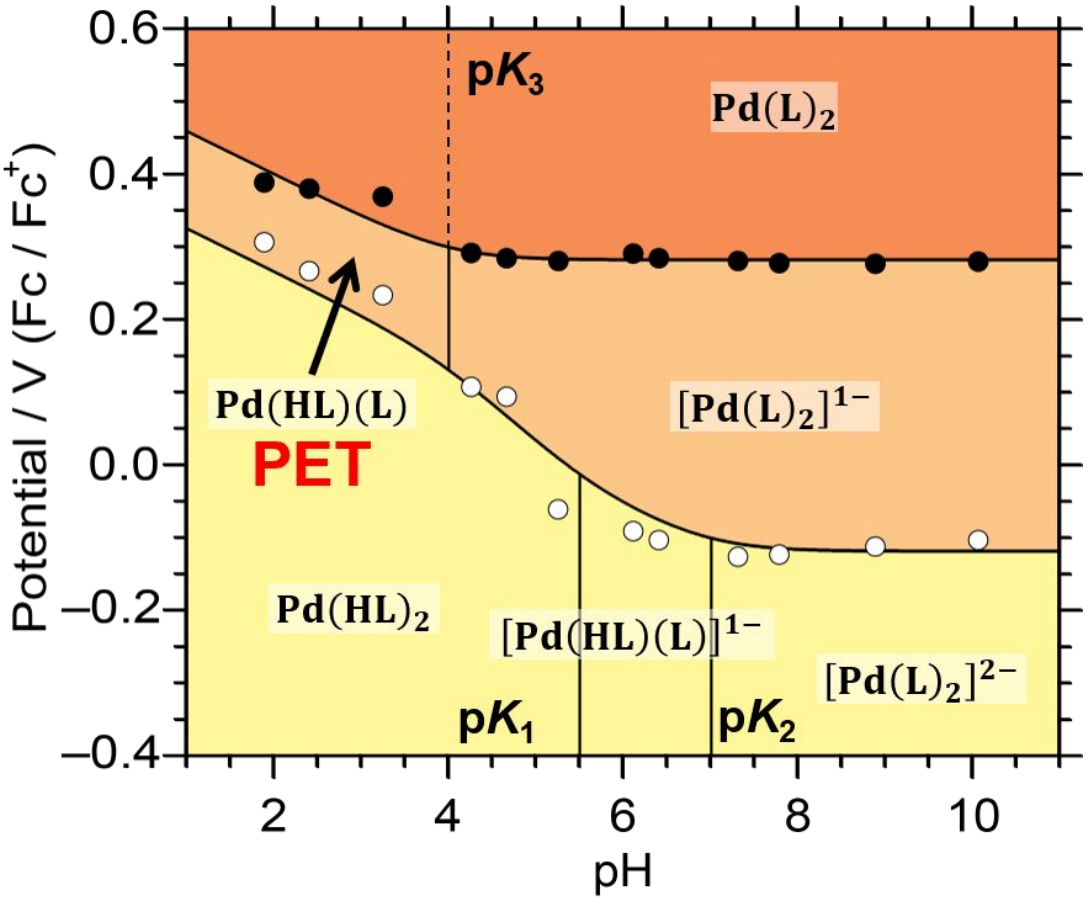

Figure S9. Pourbaix diagram of Pd complexes. Values of $E_{\mathrm{p,c}}(1)$ and $E_{\mathrm{p,c}}(2)$ were plotted by white and black circles, respectively. Solid curves overlaid by these circles are fitting results by using equations (1) and (2) in main text.

S.8 Electrochemical measurements

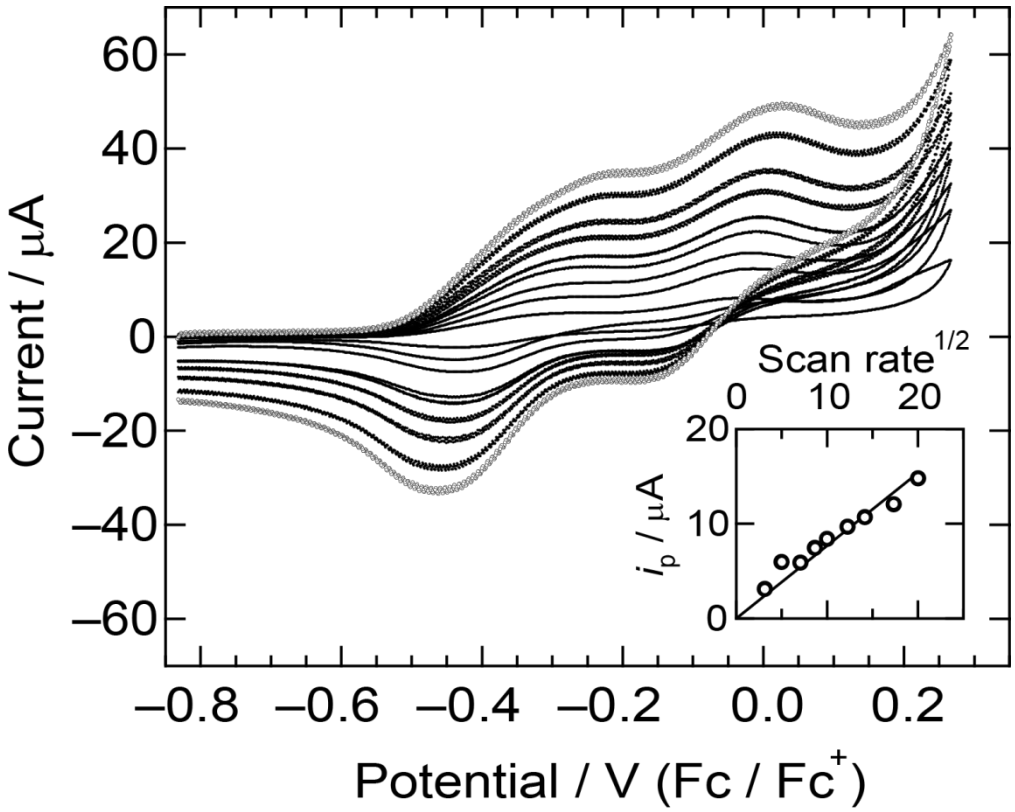

Figure S10. Cyclic voltammograms of **TBA[Ni(HL)(L)]** in 0.1 M $TBAClO_4$/DMSO solution at different scan rates (10 – 400 V s^{-1}). Inset shows a power law dependence between the peak current (i_p) and scan rate. At 100 V s^{-1}, a value of potential splitting in the first redox is 0.22 V.

S.9 NMR measurements

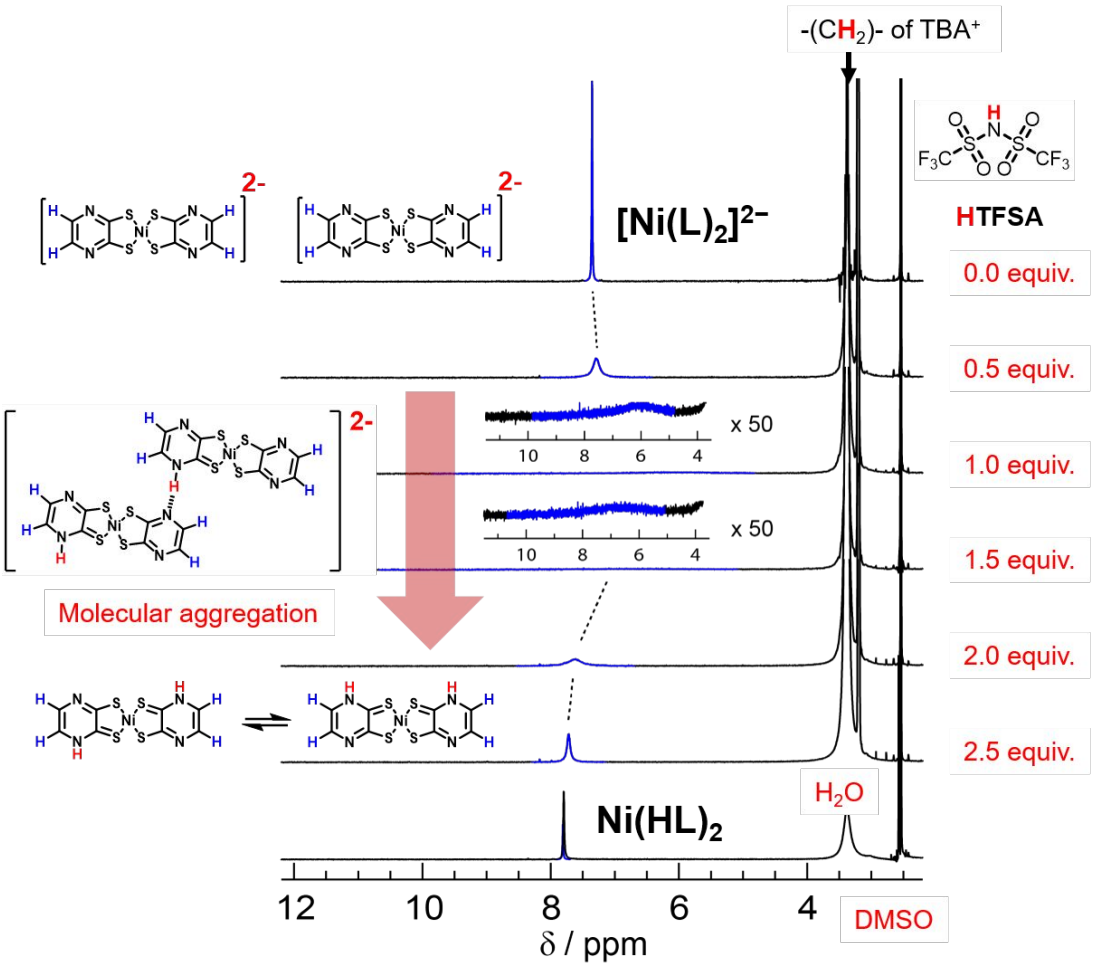

Figure S11. ^{1}H NMR signals of **$TBA_2[Ni(L)_2]$** measured in DMSO-d_6 solution under various acidic conditions. The signal from DMSO molecules (δ = 2.54 ppm) is set as a standard in all conditions. The signal before adding HTFSA corresponds to the proton at the 2,3-positions of pyrazine moieties. At the conditions of adding excess amount of HTFSA, the signal is assigned to protons of protonated pyrazine moieties, where the rapid exchange between *cis*- and *trans*-protonated structures brought out a single peak around 7.7 ppm. The bottom signal (δ = 7.80 ppm) corresponds to the proton at the 2,3-positions of pyrazine in **$Ni(HL)_2$** in DMSO-d_6, which reproduces the motional narrowing observed in the signal of **$TBA_2[Ni(L)_2]$** in DMSO-d_6 with excess amount of HTFSA.

S.10 Discussion about the MV state

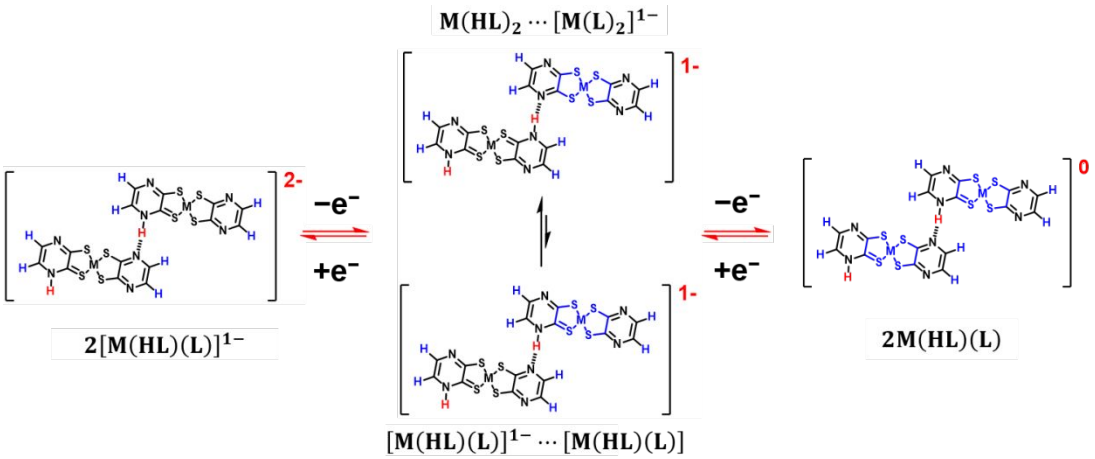

Figure S12. A schematic image of mechanism to stabilize the MV state by varying the proton coordination in H-bond. For example, an equilibrium between two kinds of H-bond dimers, **[M(HL)(L)]$^{1-}$···M(HL)(L)** and **M(HL)$_2$···[M(L)$_2$]$^{1-}$** (M = Ni and Pt), is considered as the MV state. Theoretical calculations suggest that the equilibrium is an exothermic reaction to provide the **M(HL)$_2$···[M(L)$_2$]$^{1-}$** pair in both metal complexes. The M(S_2C_2)$_2$ core of mono-oxidized species is highlighted by blue.

Table S8. Calculated sum of electronic and thermal free energies of Ni and Pt complexes

	M = Ni *E* / A.U.	M = Pt *E* / A.U.
M(HL)$_2$	-2289.364322	-2239.220189
[M(L)$_2$]$^{1-}$	-2288.237164	-2238.102536
[M(HL)(L)]$^{1-}$	-2288.729436	-2238.593561
M(HL)(L)	-2288.844535	-2238.703276

S.11 Reference

(1) Kobayashi, Y.; Jacobs, B.; Allendorf, M. D.; Long, J. R. Conductivity, Doping, and Redox Chemistry of a Microporous Dithiolene-Based Metal–Organic Framework. *Chem. Mater.* **2010**, *22*, 4120-4122.